Oxidation of Metals, Vol. 36, Nos. 1/2, 1991

The Corrosion of 6061 Aluminum Under Heat Transfer Conditions in the ANS Corrosion Test Loop

R. E. Pawel,* G. L. Yoder,* D. K. Felde,* B. H. Montgomery,* and M. T. McFee*

Received November 11, 1990; revised February 13, 1991

The corrosion of aluminum alloy fuel cladding in ultrahigh flux research reactors such as the Advanced Neutron Source may pose special temperature and structural problems associated with the buildup of reaction products during the lifetime of the core. In order to ensure that both the fuel and cladding integrity are maintained for the special conditions to be imposed on the ANS fuel plates, an experimental facility was constructed that permits the examination of material behavior for a wide range of thermal-hydraulic conditions, particularly high heat flux (to 20 MW/m^2) and coolant velocity (to 35m/sec). Tests have been conducted on specimens of 6061 aluminum that yielded meaningful comparisons to earlier data (i.e., High Flux Isotope Reactor and Advanced Test Reactor) and illustrated several important aspects of the process. In addition to the direct measurements of temperature response, these tests indicated that the film growth rate and morphology were sensitive to the heat flux and coolant water chemistry, as well as other system temperatures. The corrosion products were mainly boehmite ($Al_2O_3 \cdot H_2O$) and an iron-rich barrier-type layer on the outer surface of the boehmite, which appeared to form in certain instances as a consequence of mass transport from the cooler sections of the loop. Eventually, also depending upon the particular coolant and heat-transfer conditions, the films underwent spallation; and this event was followed by an aggressive internal reaction in the alloy underlying the film.

KEY WORDS: aluminum corrosion; 6061 aluminum; heat-transfer corrosion; corrosion in research reactors.

*Oak Ridge National Laboratory, Oak Ridge, Tennessee 37831.

0030-770X/91/0800-0175$06.50/0

INTRODUCTION

The Advanced Neutron Source (ANS) reactor core will be composed of an array of aluminum alloy clad fuel plates cooled by high-velocity heavy water. As the heat from the nuclear fuel passes through the thin cladding into the water, the high thermal conductivity of aluminum and the high heat transfer coefficient governing heat flow from the plate to the water should combine to keep the temperatures in the fuel plate at reasonable levels.

It is known, however, that the exposure of aluminum and many aluminum alloys under such conditions typically leads to the growth of an adherent oxidation product separating the fuel plate from the cooling water. At the anticipated high heat flux levels for the ANS core, the presence of this low-thermal-conductivity film may interfere with heat flow and, in certain instances, lead to excessive heating of the fuel plate. Previous experimental efforts at ORNL,[1,2] associated mainly with the High Flux Isotope Reactor (HFIR) and Advanced Test Reactor (ATR) projects, examined the corrosion behavior of several aluminum alloys in flowing, pH 5–7 water under heat transfer conditions. For heat fluxes from 3–6 MW/m^2 and coolant flow rates from 10–15 m/sec, the rate of growth of the corrosion product, boehmite ($Al_2O_3 \cdot H_2O$), was independent of these parameters and proposed to be only a function of the boehmite-coolant interface temperature and the pH of the water. The assemblage of these data, the "Griess Correlation,"[2,3] has been widely used to predict the extent of aluminum corrosion under various reactor conditions.

Since most ANS thermal-hydraulic parameters are outside the range considered by this correlation, additional information, a more extensive database and, ideally, a modified or new correlation are required. Thus, the present task was created in order to investigate the corrosion behavior of aluminum alloys under ANS thermal-hydraulic conditions, and thence to establish its effect in defining operating constraints and core lifetime. The basic objectives of the corrosion test program are: (1) to ensure that excessive fuel and clad temperatures due to corrosion product buildup do not occur during the lifetime of the ANS core (14–21 days); (2) to ensure that the corrosion/erosion processes do not compromise the structural properties and containment capabilities of the fuel cladding; and (3) to provide specifically a means for predicting the time-dependent oxide thickness during an ANS fuel cycle. Because of its long history of satisfactory performance as a fuel cladding in experimental reactors, 6061 Al (nominal composition, wt.%: 0.6 Si; 1.0 Mg; trace Fe, Cr, Mn) is the present choice for the ANS. Our main series of experiments is focusing on this alloy.

EXPERIMENTAL PROCEDURES

The Test Loop

The Corrosion Test Loop facility, described in earlier reports,[4,5,6] has been in virtually continuous operation since its installation in January 1988. Briefly, the test facility is a forced-flow water loop fabricated entirely of 304L stainless steel components, capable of pressurized operation to 7 MPa and coolant water flows to 2 L/sec. The specimen consists of an aluminum alloy tube forming a rectangular flow channel that is equivalent in gap width to that of the ANS coolant channels. A drawing of the main section of the specimen is presented in Fig. 1. The specimen is surrounded by insulation and pressure backing (not shown in the figure), welded to large electrodes, and attached to the main section of the loop so that coolant velocities in the specimen channel up to 35 m/sec ($Re > 1 \times 10^5$) can be achieved. A simplified schematic drawing of the test loop system is shown in Fig. 2. The heat flux (up to >20 MW/m^2) is produced by self-resistance heating of the specimen, where the irregular cross-section concentrates the heat flux to the desired central region. Approximately 80% of the heat is generated in the thick central region of the specimen. The power is furnished by a 30 kA dc power supply and, downstream of the specimen, the heat is removed by a water-cooled heat exchanger. System pressure is maintained in the high-pressure

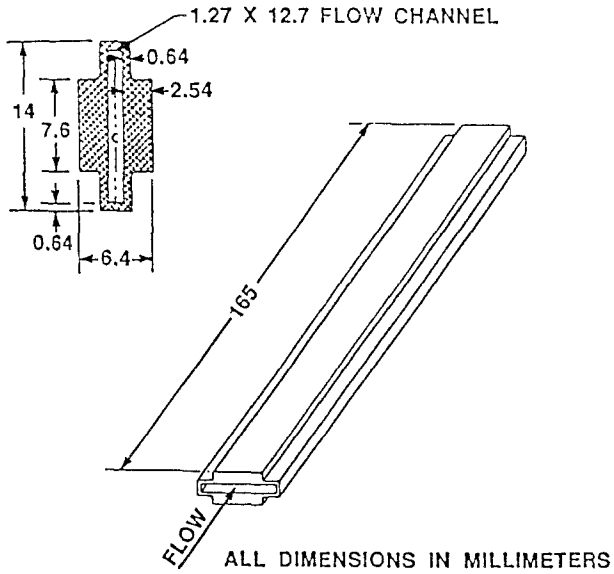

Fig. 1. Central section of corrosion test specimen.

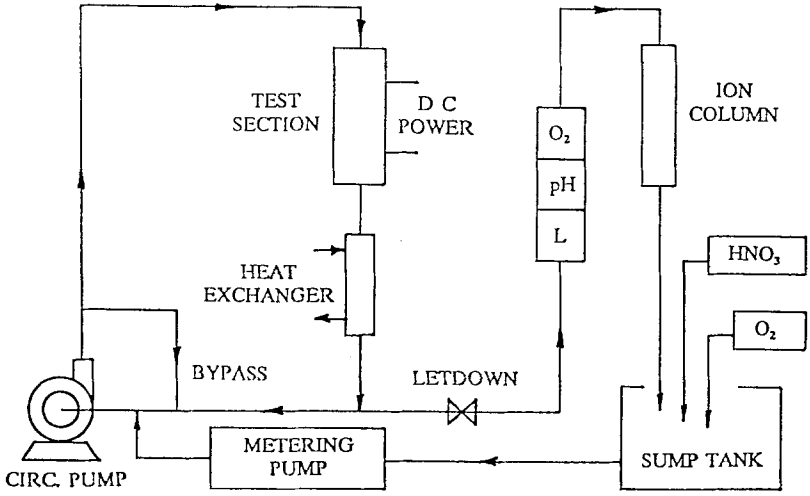

Fig. 2. Schematic diagram of ANS Corrosion Test Loop.

circulation loop (4 MPa at the specimen inlet) by allowing a small, continuous water flow through a moderated letdown valve to a low-pressure secondary loop, where instrumentation and equipment for maintaining suitable water chemistry are located. Makeup water flow is provided by a high-head, positive displacement pressurization pump. The coolant circulation system in the loop is similar to that employed in many research reactors.

The outer surface of the main section of the specimen (see Fig. 1) is instrumented along its central axis with ungrounded, stainless steel sheathed (0.5 mm), type N thermocouples. Seven thermocouples are arranged axially 25.4 mm apart on one side; three are located on the other side to provide additional measurements and comparisons. The three "reference positions" on the specimen, which will be noted in subsequent discussions and figures, coincide with three of these thermocouple locations along the specimen: Position 4 is the axial midpoint of the specimen, with Positions 2 and 6 located about 51 mm from this point toward the coolant entrance and exit ends, respectively. Thus, because the coolant temperature increases as the specimen is traversed, the severity of the oxidation reaction also increases from Position 2 to Position 6.

For a given level of electrical power supplied to the specimen and a given coolant flow rate, a temperature profile along the specimen is established. If the loop's thermal-hydraulic parameters are then held constant, changes in the measured temperatures along the outer part of the specimen can be related quantitatively to the buildup of oxidation products at the specimen-coolant interface. At the high heat fluxes involved in this work, temperature increases from this source in excess of 100 K are not uncommon.

Fabrication of a test section for each loop test requires precision electron-beam welding of two carefully prepared specimen halves (to form the shape shown in Fig. 1), followed by conventional gas-tungsten-arc welding of the completed specimen to the massive electrodes. Procedures for accomplishing the welding, instrumentation, and other assembly steps have been developed and improved throughout the program.

The loop operates under computer control of the electrical and coolant flow parameters, including various safety features. The associated data acquisition system (DAS) records all temperatures, pressures, flow rates, power levels, and water properties at designated time intervals. While, in principle, the test loop and its support equipment are uncomplicated, integrated operation at the required performance level has entailed continuous attention to the various components. In particular, a significant amount of time and effort has been expended on the measurement and control of the pH and conductivity of the coolant water in the loop.

Measurements and Calculations

The ANS Corrosion Test Loop Facility provides the means to expose an aluminum surface to rapidly flowing coolant under heat transfer conditions. During a test, the electrical power generated in the specimen and the coolant conditions are generally held constant, so that *changes* in temperature of the specimen at its outer, insulated side are mostly from increases in the thermal resistance in the heat path due to the growth of the corrosion product at the metal–coolant interface. While these changes, per se, are important observations in that they imply similar increases in the fuel temperature in the ANS core, they are also useful in obtaining the oxide thickness and growth kinetics through established heat transfer and thermal-hydraulic calculations. Certain results and implications of these calculations can be checked by observations and measurements on the reacted specimen surface at the completion of the experiment, but the important results are basically all calculated quantities.

The electrical heat generated in the aluminum and rejected to the coolant results in normal, transverse, and axial temperature gradients within the specimen. While a relatively steep gradient exists across the specimen to the coolant, particularly near the metal–oxide interface, the temperatures also increase uniformly from the coolant inlet end to the exit. Thus, the temperature dependences of the physical properties of the 6061 Al must be considered in all calculations. An important consequence of the axial gradient is that (for a constant average power) the heat flux is larger at the hot end and smaller at the cooler end of the specimen. As the reaction products thicken more rapidly at the hotter end, the range of heat flux over the specimen

length increases during an experiment. Only at a position near the axial midpoint will the heat flux remain essentially constant for the complete test. Tests were commonly continued for a maximum time of 21 days, or were stopped earlier if it was recognized that spallation of the product film had commenced at the hotter portion of the specimen.

Despite these complexities, it is possible, in principle, to utilize the continuous measurements of specimen temperatures and the controlled loop parameters to calculate the growth rates of the corrosion products along the specimen and to correlate these rates with the local conditions. Several computational schemes were examined,[7] and two computer programs are now in use. The programs, OXCAL and ANSDAT, were written completely independently but exhibit satisfactory agreement in the computed quantities.

RESULTS AND DISCUSSION

It is not the intent of this paper to include a detailed discussion of the individual experiments. However, to furnish a credible picture of the important oxidation behavior as well as to summarize the status of our investigation, a general account of the results and their significance is in order.

Film Growth Kinetics

In virtually every experiment, the temperature of the specimen at each point along its central axis (and the calculated product film thickness) increased at a slightly decreasing rate that was eventually recognized to depend on several of the system variables. In experiments exhibiting comparatively high rates of film growth, or ones allowed to run for sufficiently long periods of time, partial spallation of the film was commonly initiated at the hotter end of the specimen, which resulted in a perturbation of the local heating. In order to provide for more complete postexperiment examinations, the tests were terminated before spallation had progressed over the entire specimen length.

An example of this behavior is shown in Fig. 3, which depicts the oxidation rate curves calculated for three points along the specimen for CTEST No. 4. (As noted earlier, Positions 2, 4, and 6 are located 50 mm apart about the axial midpoint at fractional length positions L/6, L/2, and 5L/6 from the coolant inlet end.) The conditions of the experiment and the local parameters are listed on the figure. The parameters include the coolant velocity (V_c), average heat flux (ϕ_{avg}), inlet and outlet coolant temperatures (T_{ci} and T_{co}), local coolant temperature (T_c), and oxide-coolant interface temperature ($T_{x/c}$). The rates of film growth are measurably higher than

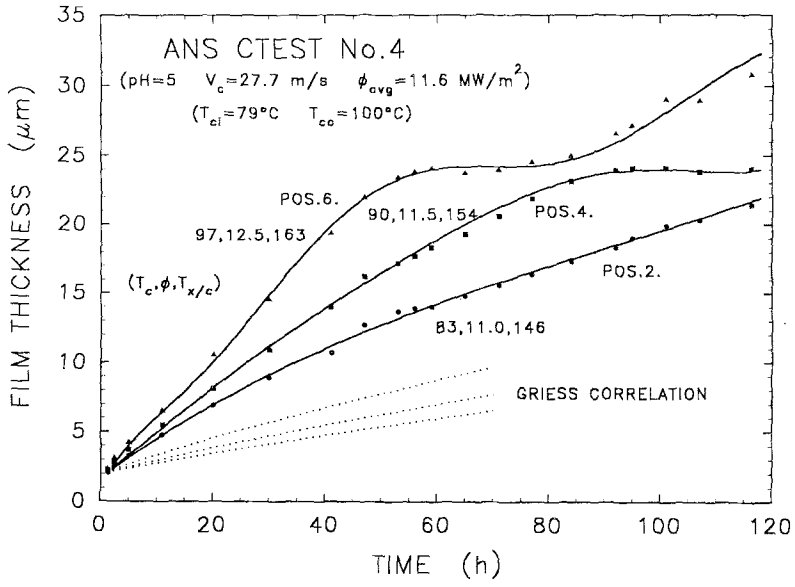

Fig. 3. Film growth on 6061 Al for CTEST No. 4 at the three reference positions on the specimen (see text). Growth rates predicted by the Griess Correlation are also shown for comparison.

those predicted by the Griess correlation[2] for these oxidation conditions. This correlation expresses the film growth in pH 5 water solely in terms of the interface temperature, $T_{x/c}$, as

$$x = (1.125\text{E}4)t^{0.778} \exp(-4600/T_{x/c}) \tag{1}$$

where

x = film thickness, μm

t = time, hr

$T_{x/c}$ = interface temperature, K

From the rate curves in Fig. 3, an indication of spallation was observed at positions 6 and 4 after about 55 and 90 hr, respectively, when the apparent thickness of the film approached 25 μm. CTEST No. 3, conducted under similar heat flux and coolant conditions except at pH 6, produced comparable behavior but with even more rapid reactions. X-ray identification of the films on the reacted Al surfaces indicated that the major product was boehmite or "pseudo-boehmite," a poorly or micro-crystalline form.

CTESTS Nos. 6 and 7 showed that the corrosion rates were dramatically reduced for almost identical thermal-hydraulic conditions by controlling the

pH of the coolant to 4.5 rather than 5.0. In addition, the posttest appearance of these specimens was characterized by a straw-reddish-brown film that increased in intensity from inlet to outlet end. This film, shown to be mainly an iron-rich layer on the outer surface of the boehmite, appeared to function as an efficient diffusion barrier, thus reducing the rate of reaction. Its location solely on the outer surface was consistent with the idea that the primary mechanism of boehmite growth was anion diffusion and that the source of iron was *not* from the 6061 alloy itself.

A series of tests appropriate for certain ANS core-specific applications was also undertaken. Simply, these tests were conducted at pH 5 with heat fluxes and coolant flows comparable to the previous tests, but with the coolant inlet temperature adjusted to give lower local coolant temperatures. Perhaps surprisingly, the rates of film growth for most of these tests were low, often even lower than those predicted by the Griess correlation. It was generally observed that the iron-rich layer was also found on these specimens unlike, for example, CTEST No. 4, where no layer was observed and the film growth rates were high. Low coolant temperatures as well as low coolant pH's favored the appearance of the iron-rich layer, and both were associated with low film growth rates.

An example of the film growth kinetics for experiments involving a range of thermal-hydraulic conditions is shown in Fig. 4. For the tests shown, the oxide-coolant interface temperatures were nominally the same; however, the coolant inlet temperature, the local coolant temperature, and the heat flux were varied as indicated in the figure. The range of rate predictions on the basis of the Griess correlation,[2] which depends only upon the interface temperature, is shown for comparison. Clearly, the other system parameters are exerting an influence, and the Griess correlation should not be—nor was it intended to be—used outside the range of data upon which it was based. From these and other tests, we have found that higher heat fluxes, interface temperatures, and oxide temperatures all lead to more rapid film growth; lower coolant temperatures (both within the test section and in the remainder of the loop) and lower coolant pH lead to lower rates of film growth; and, as noted above, the latter parameters appear to favor the formation of an Fe-rich layer on the oxide surface that is also associated with the lower film growth rates.

A surprising additional conclusion from the series of tests was that the coolant inlet temperature was apparently an *independent* variable affecting the oxidation process. A specific comparison for two sets of rate data illustrating this point is shown in Fig. 5, where the two groups of thermal-hydraulic test conditions listed on the figure are essentially identical except for the 12° difference in the coolant inlet temperature. Along with the observed difference in the film growth rate, the surface of CTEST No. 13(6)

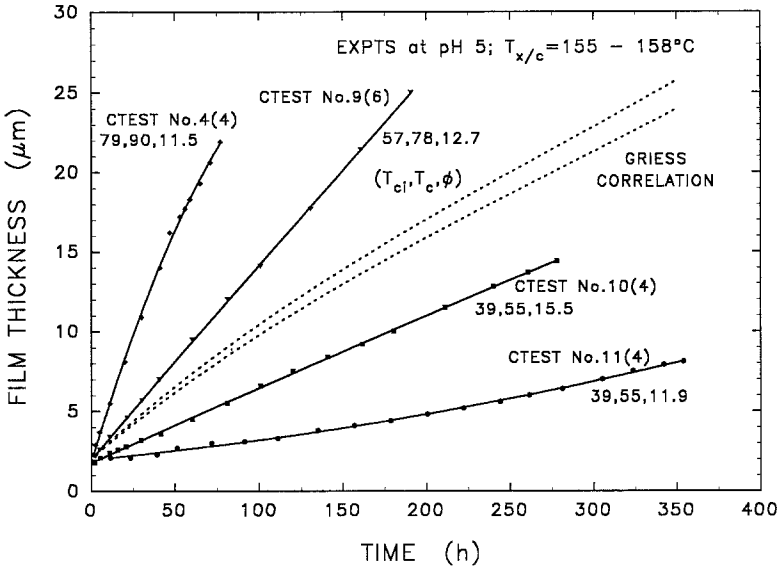

Fig. 4. Film growth observed during CTESTS for specimens having near-identical interface temperatures, $T_{x/c}$. For a given experiment, the particular position along the specimen is noted in parentheses; coolant temperatures and heat fluxes are as indicated.

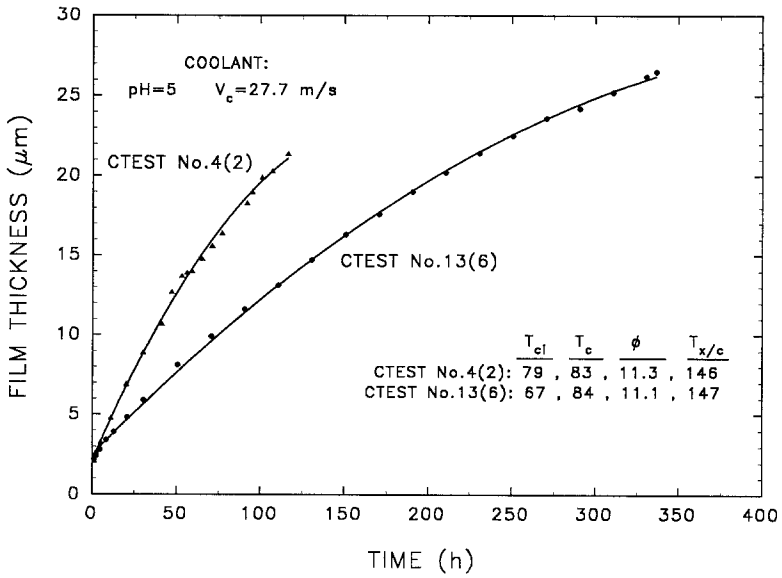

Fig. 5. A comparison of film-growth data illustrating the importance of the coolant inlet temperature, T_{ci}, as an "independent" variable.

(read CT-13, position 6) showed evidence of the Fe-rich layer, while that of CTEST No. 4(2) did not (or at least showed much less). A possible mechanism for the formation of this layer is discussed below.

The highest average heat flux utilized in this program to date was 18.7 MW/m^2 in CTEST No. 16. In this experiment, the comparatively large axial temperature gradient along the specimen caused significant variation-with-position and changes-with-time in the local heat flux and, thus, in the interface temperatures along the specimen. For example, as shown in Fig. 6, the heat flux at position 6 changed from 19.4 MW/m^2 early in the experiment to 21.1 MW/m^2 near the end. As the average power is maintained at a constant level, decreases in the heat flux were observed at position 2. While not apparent from the figure, spallation was found at the hot end of the specimen at the conclusion of the experiment. Compared to CTEST No. 4 (in Fig. 3), CTEST No. 16 was characterized by substantially higher heat fluxes and interface temperatures, factors that govern the effective temperature of the growing oxide film. The slower rates of film growth demonstrate the benefit of the low coolant temperatures suggested above.

Data Treatment and Analyses

Several analytical expressions for describing the oxidation kinetics have been investigated. An inherent difficulty in applying commonly used oxidation models to the present experimental data is that the system is not

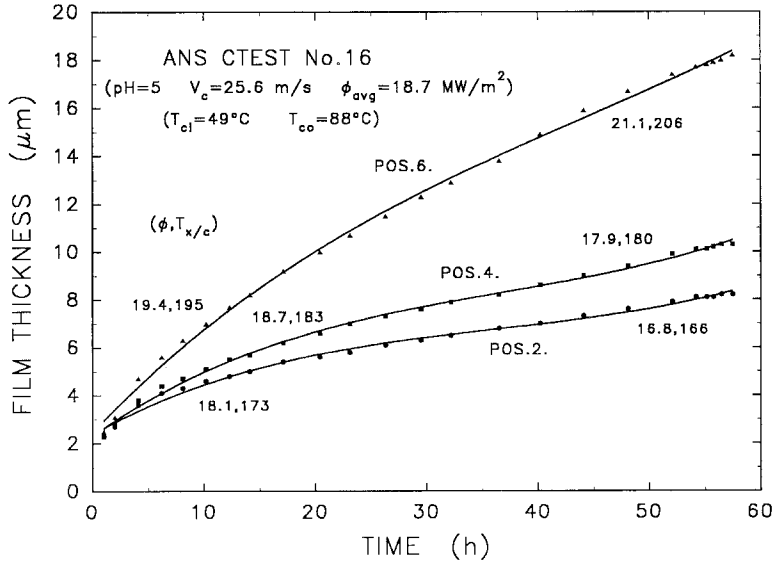

Fig. 6. Film growth for CTEST No. 16, conducted with an average heat flux of 18.7 MW/m^2.

completely isothermal. While the average power and coolant temperatures are held constant during an experiment, the heat flux passing through the growing oxide film creates a continuously increasing temperature in the oxide. Thus, the growth rates are not expected to follow those dictated by simple rate laws, even if the same diffusion-related mechanism applies.

At the present time, we have not defined a sophisticated oxidation model that is consistent with the observed behavior. However, in order to facilitate quantitative comparisons of the oxidation kinetics for different thermal-hydraulic conditions, and to serve as the basis of preliminary correlations,[8] an empirical approach was taken (at least in regard to the changing oxide temperatures).

From our data sets, it has been observed with few exceptions that the thickness of the product film at a given point on the specimen increases at a slightly decreasing rate. While it was apparent that ideal "parabolic" growth was not occurring, associated at least in part with the reason cited above, the normal shape of the curves seemed consistent with the common general rate equation

$$\frac{dx}{dt} = \frac{k}{x^n} \tag{2}$$

where

x = film thickness, μm

t = time, hr

k = rate constant, $\mu m^{n+1}/hr$

n = constant (mechanism number)

Many oxidation systems seem to follow this simple rate equation, with $n = 1$ or 0 (accounting for parabolic or linear growth). The kinetic result of complicated changes in diffusion behavior in a growing film can often be empirically accounted for by noting that $n \neq 1$ and/or is time-dependent. Similarly, the influence of changing film temperatures as in the present experiments can be practically accounted for in this manner. It is significant to note that the Griess correlation also invoked this form of analysis.

The integrated equation takes the form

$$x_t = [x_0^{n+1} + (n+1)kt]^{1/(n+1)} \tag{3}$$

where

x_t = film thickness at time, t

x_0 = film thickness at time $t = 0$

On the basis of this equation, our data to date yield a best value for the time exponent, $1/(n+1)$, of 0.74 ± 0.07. Thus, the shape of our growth rate curves is essentially identical to that of Griess,[2] who reported a growth exponent of 0.778. However, as noted earlier, our values of the rate constant have been observed to depend on several system parameters rather than only one (the oxide-coolant interface temperature) as proposed by Griess. For assigned values of the coolant pH = 5, coolant inlet temperature = 312 to 322 K, and coolant velocity = 25 to 26 m/sec, a "preliminary correlation" was recently proposed[8] that defines the rate constant k as a function of the local coolant temperature and heat flux

$$k = 6.992\text{E}5 \exp[-7592/(T_c + 10\phi)] \ \mu\text{m}^{1.351}/\text{hr} \tag{4}$$

where

T_c = local (bulk) coolant temperature, K

ϕ = local heat flux, MW/m^2

The requirements and restrictions for using Eq. (4) are clear. Nevertheless, it presently represents a useful basis for calculations and comparisons of film growth behavior.

Oxidation Product Analysis

The physical, chemical, and structural characterization of the product film found on the reacted specimens was undertaken by several techniques. On various specimens, we have employed standard metallographic procedures, scanning and transmission electron microscopy (SEM and TEM), x-ray structural analysis, energy dispersive x-ray analysis (EDX), and electron microprobe analysis. Simply, for "rapidly growing films" (without the Fe-rich layer), the product was generally a film of reasonably uniform thickness, virtually transparent to the naked eye, and identified as boehmite ($Al_2O_3 \cdot H_2O$) typically from thicker, hotter parts of the specimen, and/or pseudo-boehmite from the thinner, cooler regions. No other form of oxide or hydrated oxide has been identified as a prevalent reaction product, although small proportions of bayerite, $Al_2O_3 \cdot 3H_2O$, were commonly observed along with the boehmite. On many specimens, particularly those from tests showing comparatively slow film growth rates, a distinguishing feature of the product layer was a straw discoloration noted earlier to be an iron-rich layer. In their early stages of growth, these films were often quite irregular in thickness; thicker films were more uniform. A complete identification of the components in these films has not yet been made, but it

appeared from the x-ray diffraction results that boehmite and pseudo-boehmite were also the main constituents, along with additional weak lines due to an additional phase (or phases).

The iron-rich layer was found by EDX and electron microprobe work to be limited to the outer 5 or 10% of the film. It was comprised not only of Fe (and Al and O), but had lesser amounts of Cr and lesser still of Si, all occupying the outermost regions. Additional analyses will be required to define the chemical and structural species involved, but the film may well be a complex Fe–Cr oxide of some sort rather than a Fe–Cr-enriched boehmite. We were not able to identify α-Fe_2O_3, hematite, as earlier reported as a minor component in similarly appearing films formed on aluminum cladding in-pile.[9]

The fact that the Fe, Cr, and Si congregate on the outer surface, with none being observed in the inner portions of the film, suggests that the source of these metals is not the aluminum alloy itself but some other component of the loop system. The lack of mixing of this layer also is consistent with the premise that the mechanism of oxidation is one involving anion diffusion, perhaps of oxygen or hydroxyl ions, within the boehmite. Mass transport of material in loop-type systems is a common occurrence, but its importance to the formation of this particular layer is speculative, particularly in light of the observation that the Fe concentration in the cooling water was consistently less than 20 ppb. However, the general characteristics of the solubility of metal oxide species as a function of pH and temperature do suggest a possible mechanism.

If the iron (and chromium) species exhibit a typical retrograde solubility, particularly at coolant pH levels of 5 and below, then this particular driving force will exist to provide transport from the cooler stainless steel parts of the loop to the hotter aluminum specimen. In accord with this concept, it is observed that a lower pH (4.5) strengthens the Fe-rich layer and further retards the rate of boehmite growth (at lower pH, the solubilities at both extremes of temperature are increased and also, presumably, their difference). In addition, the emergence of the coolant inlet temperature as an independent variable supports the mass transport mechanism, since T_{ci} is indicative of the coolant temperature in the stainless steel part of the test loop. Thus, the oxidation characteristics in these tests, and probably also in a reactor system, may be complicated by the existence of a two-layer oxidation product, each with different diffusion properties.

Spallation and Internal Reactions

For the experimental conditions under consideration here, spallation is the flaking or sloughing of some significant fraction of the boehmite layer;

only occasionally does it result in virtually complete oxide removal in isolated areas of the specimen surface. Spallation of the boehmite from exposed 6061 aluminum alloy specimens was observed in many tests that produced films with or without the Fe-rich overlayer. Spallation was always initiated at the hot (coolant exit) end of the specimen and the spall front progressed down the specimen for longer exposures. Each experiment was terminated before the entire specimen had spalled, leaving a comet-shaped pattern that clearly identified the spalled and unspalled regions. Occasionally, the onset of spallation was positively discerned from measured temperature changes or from a slope change in the rate curves sometimes followed by a decrease in the apparent film thickness, as in Fig. 3. Alternately, as in Fig. 6, little indication of this type of change was observed, and spalling could not be confirmed until the test section and specimen were disassembled.

While at first glance spallation appears to offer some potential benefits for improved heat transfer in the system, it has been found here, and earlier by Griess,[1,2] that spallation in the 6061 alloy is associated with the onset of extensive internal reactions beneath the oxide. Metallographic inspection of cross-sections of such specimens revealed severe attack within the metal underlying the spalled film. An example is given in Fig. 7, which shows cross-sections from an unspalled and a spalled region of the same specimen. The top part of the figure exhibits a reasonably uniform layer (of boehmite) about 20 μm thick overlaying the 6061 Al. The lower part, from a downstream section of the same specimen, shows the irregular spalled film and, in the metal, the beginnings of the internal reaction zone. The depth of this zone, which seems to be composed of oxide material and perhaps voids (or bubbles) located on grain boundaries and within the metal grains, is perhaps 0.1 mm in this instance, but in other cases has been observed to be much larger and the attack more severe. Such a case is illustrated in Fig. 8, which clearly shows both grain boundary and intragranular attack, as well as apparent voids and internal reaction products. Similar behavior in ANS fuel cladding would be unacceptable. No internal reaction zones were observed beneath unspalled films, even when examined by TEM,[10] thus implying that these features were a result of spallation rather than the cause.

From our experimental temperature measurements during the tests, and from postexperiment observations, spallation was estimated to occur when the calculated film thicknesses were between about 28 and 17 μm for heat fluxes from 12–20 MW/m^2. The corresponding range of temperature drops across the films (due to the heat flux) was approximately 120–150 K. It was evident that at higher heat fluxes, spallation of thinner films occurred. If a true inverse relationship applied, a constant value for the temperature drop at the time of spallation would exist. Consistent with this premise, Griess's earlier work[1,2] reported spallation for several alloys at about 50 μm for a

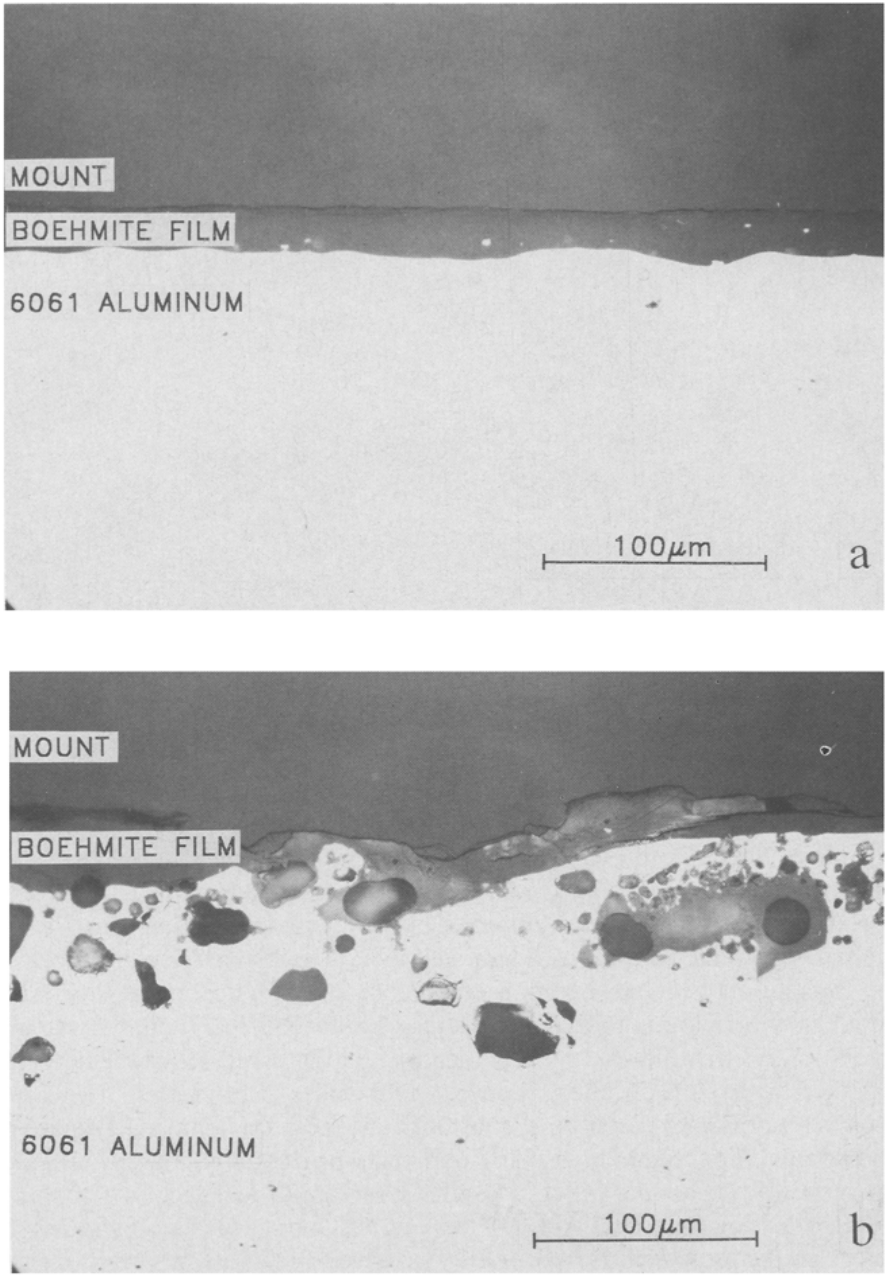

Fig. 7. Cross-sections of CTEST specimen showing (a) the unspalled boehmite layer, and (b) a spalled region showing the remnants of the layer and the early stages of growth of the internal reaction zone.

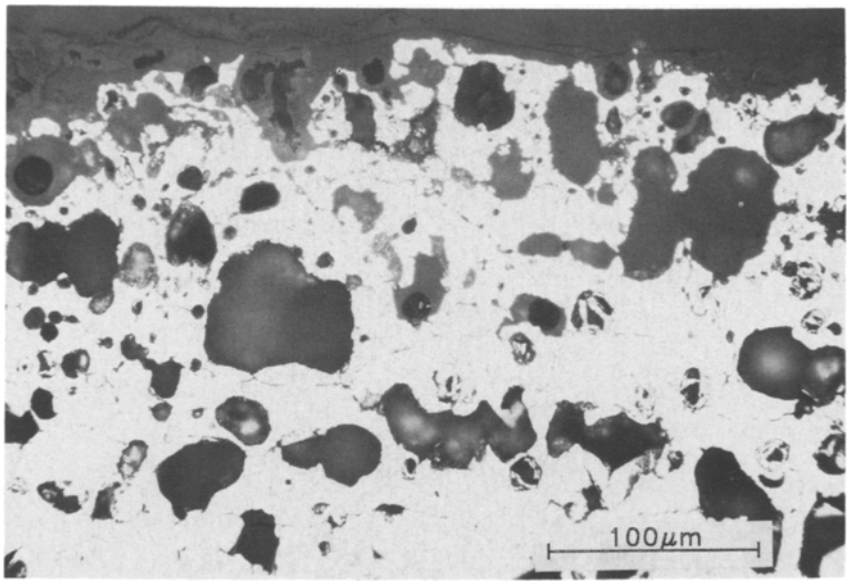

Fig. 8. Cross-section from CTEST specimen exhibiting a large amount of internal reaction. Note attack along grain boundaries as well as within the grains.

lower heat flux and coolant velocity, so that roughly the same temperature drops were involved. It thus appeared from these observations that for the growth of boehmite on 6061 Al under "steady-state" oxidation conditions, spallation would not be expected until the temperature drop across the oxide film exceeded 120 K. We should note, however, that oxidation under other thermal-hydraulic conditions might well affect this provisional criterion.

Spallation of an oxide film is recognized as a physical process brought about by the buildup of mechanical stresses in the system. In many systems, spallation is often induced by rapid changes in temperature, where differential thermal expansion effects between film and substrate exist. However, even for isothermal conditions, substantial stresses that cause deformation and spalling are common to many oxidation processes. Generally, stresses can arise during oxidation as a result of (a) epitaxial effects, (b) volume changes during reaction, and (c) the establishment (or the changing) of defect gradients. Of course, there are also several mechanisms besides spallation by which these stresses may be relieved, so that the level of stress, and its significance to the oxidation behavior, depends upon a competition between stress generation and stress relief. The precise mechanism of oxidation is also important.

Although epitaxial stresses are thought to be small, the other mechanisms remain as reasonable possibilities by which mechanical stresses in a growing boehmite film may increase to the point where spallation occurs, but the precise manner by which the heat flux or the temperature gradient influences this process is not presently obvious. In fact, an argument can be made that stresses arising solely as a consequence of the temperature gradient in the growing boehmite film would be small. In our experiments at constant average power, the oxide at the oxide–coolant interface is always at the same temperature ($T_{x/c}$ does not change much). For an anion diffusion mechanism of oxidation, which we think is the dominant mechanism, the oxide forms at the oxide–metal interface, which is at a higher temperature that increases as the film grows. Thus, an increment of oxide has a larger lattice parameter than that of the previously formed increment. But because each of these incremental layers remains at a temperature at or near that at which it formed, there is little, if any, elastic stress that is a direct result of the temperature difference (analogous to the stress state in an unconstrained film with an imposed temperature gradient). Thus, in the absence of other stress-generating mechanisms, each increment of layer growth can be visualized as developing essentially stress-free and then remaining so because the temperature of each increment does not change. It is recognized that some stresses in the film could, in fact, arise as a result of the temperature gradient, because the real oxidation scenario is not completely ideal. While the magnitude of these stresses would certainly be smaller than those calculated to arise by taking a grown film, constraining it in some way, and then establishing a temperature gradient, they might nonetheless be large enough to cause fracture. Additionally, if the oxidation mechanism were one of cation diffusion (or even partially cation diffusion) in the boehmite, a mechanism for thermal stress generation could arise because of the changing temperatures of the growth increments. However, the complete stress description in this instance would be more complicated.

It is significant in this discussion to observe that spallation was not induced in several experiments where the power (and hence, temperatures and temperature gradients across the oxide) was cycled during and at the end of the test. However, in regions of the specimen where spallation had already occurred, some additional spallation likely took place. While these tests were not conducted under extremely rapid rates of temperature change, they nevertheless point out that boehmite films on aluminum can at least survive moderate temperature changes. These results are in general accord with those of Griess,[2] who observed spallation on temperature cycling only if the oxide was thicker than a certain value ($x > 25\ \mu m$) approaching the thickness at which spallation under steady-state conditions was normally observed. These experiments indicated also that when spallation during

cycling did occur, it was as a result of the rapid reheating part of the cycle. Slow heating over a few minutes time did not initiate spallation.

The tolerance of the boehmite layers to the effects of differential thermal expansion does suggest that the mechanism of stress generation leading to spallation may be found elsewhere, and indeed may be somehow associated with the heat flux, the temperature gradient in the oxide, or perhaps some aspect of hydrogen injection at the oxide metal interface. For example, Draley and Ruther,[11-13] in their classic experiments on corrosion of aluminum in high temperature water, concluded that atomic hydrogen becomes available at the oxide–metal interface and, depending upon the temperature, either diffuses into the metal or back through the oxide to the coolant. Combination of the hydrogen at local sites in either instance could lead to high-pressure, potentially disruptive gas bubbles. While it is reasonable to relate some of the features in Fig. 8 to this mechanism, in fact, bubbles, incipient bubbles, or other evidence of hydrogen damage were not found upon TEM examination of the aluminum beneath a boehmite film just prior to spallation. Thus, there is no direct evidence here that this mechanism causes spallation but, perhaps conversely, it appears that spallation may enhance subsurface hydrogen activity, blistering, and internal reactions.

SUMMARY AND CONCLUSIONS

1. A test loop was constructed for investigating the corrosion of aluminum alloys under high heat fluxes (up to 20 MW/m^2) and coolant water velocities (up to 35 m/sec). The features of the loop are very similar to the flow system through the core and heat exchangers of a typical water-cooled research reactor. The loop was used to study the reaction of 6061 aluminum for a range of thermal-hydraulic conditions appropriate for fuel cladding in the ANS reactor core.
2. The rate of growth of the oxidation product (mostly boehmite, $Al_2O_3 \cdot H_2O$) on 6061 Al surfaces was observed to depend upon heat flux and coolant water chemistry, as well as on the coolant and interface temperatures. High heat fluxes, interface temperatures, and oxide temperatures all lead to rapid film growth; lower coolant temperatures, both within the test specimen and in the remainder of the loop, lead to lower rates of growth. The latter parameters favored the formation of the iron-rich layer (see below), which was also associated with lower oxide growth rates. An empirical oxidation rate expression was developed that accounts for the key features of the observed kinetics and that is useful as a basis for calculations and comparisons of film growth.

3. An iron-rich layer often formed on the outer surface of the boehmite film, particularly when lower coolant inlet temperatures and lower coolant pH's were used. The layer appeared to function as a diffusion barrier, lowering the overall rate of film growth. We hypothesize that the mechanism by which it formed was one of mass transport of iron and (chromium) oxide species from the stainless-steel components of the loop.
4. Spallation of the boehmite film occurred during steady-state (constant power) experiments at film thicknesses that depended (inversely) upon the heat flux or some other related parameter. Spallation under these particular conditions was not observed until the temperature drop across the growing oxide exceeded 120 K.

ACKNOWLEDGMENTS

This research was sponsored by the Division of Materials Sciences, U.S. Department of Energy, under contract DE-AC05-840R21400 with the Martin Marietta Energy Systems, Inc.

The authors appreciate the many contributors to the ANS Corrosion Loop Program at Oak Ridge National Laboratory. Fabrication of the test sections and their posttest examinations have involved J. F. King, J. D. Hudson, J. D. McNabb, and D. W. Swaney of the Materials Joining Group; R. R. Steele, O. B. Cavin, and T. J. Henson from the High Temperature Materials Laboratory; and L. D. Chitwood from the Nondestructive Testing Group. Special thanks are due to J. A. Crabtree for data-handling, and to W. R. Gambill, R. E. Mesmer, J. C. Griess, C. D. West, and D. L. Selby for their continuing interest and helpful suggestions. D. F. Wilson and G. E. C. Bell provided a critical review of the manuscript.

REFERENCES

1. J. C. Griess *et al.*, *Effect of Heat Flux on the Corrosion of Aluminum by Water. Part III. Final Report on Tests Relative to the High-Flux Isotope Reactor* (ORNL-3230, Oak Ridge National Laboratory, Oak Ridge, Tennessee, December 1961).
2. J. C. Griess, H. C. Savage, and J. L. English, *Effect of Heat Flux on the Corrosion of Aluminum by Water. Part IV. Tests Relative to the Advanced Test Reactor and Correlation with Previous Results* (ORNL-3541, Oak Ridge National Laboratory, Oak Ridge, Tennessee, February 1964).
3. R. E. Pawel, *On the Kinetics of the Aluminum-Water Reaction during Exposure in High-Heat Flux Test Loops. I. A Computer Program for Oxidation Calculations* (ORNL/TM-10602, Oak Ridge National Laboratory, Oak Ridge, Tennessee, January 1988).
4. D. L. Selby, R. M. Harrington, and F. J. Peretz, *Advanced Neutron Source (ANS) Project Annual Report. April 1987–March 1988* (ORNL/TM-10860, Oak Ridge National Laboratory, Oak Ridge, Tennessee, February 1989).
5. D. L. Selby, R. M. Harrington, and F. J. Peretz, *Advanced Neutron Source (ANS) Progress Report* (ORNL-6574, Oak Ridge National Laboratory, Oak Ridge, Tennessee, April 1990).

6. B. H. Montgomery, R. E. Pawel, and G. L. Yoder, *Trans. Am. Nuc. Soc.* **57**, 300 (1988).
7. R. E. Pawel and D. W. Yarbrough, *Modeling Heat Generation and Flow in the Advanced Neutron Source Test Loop Specimen* (ORNL/TM-10603, Oak Ridge National Laboratory, Oak Ridge, Tennessee, January 1988).
8. R. E. Pawel *et al.*, *The Development of a Preliminary Correlation of Data on Oxide Growth on 6061 Aluminum under ANS Thermal-Hydraulic Conditions* (ORNL/TM-11517, Oak Ridge National Laboratory, Oak Ridge, Tennessee, June 1990).
9. V. A. Walker, M. J. Graber, and A. W. Gibson, *ATR Fuel Materials Development Irradiation Results, Part II* (IDO-17157, Idaho National Engineering Laboratory, Idaho Falls, Idaho, June 1966), p. 90.
10. K. Farrell (personal communication of unpublished results, Oak Ridge National Laboratory, Oak Ridge, Tennessee, March 1989).
11. W. E. Ruther (personal correspondence, November 7, 1988).
12. J. E. Draley and W. E. Ruther, *Proceedings of the International Conference on the Peaceful Uses of Atomic Energy*, Vol. 9 (Geneva, August 1955), p. 391.
13. J. E. Draley and W. E. Ruther, *J. Electrochem. Soc.* **104**, 329 (1957).